Nuclear Instruments and Methods in Physics Research A 753 (2014) 61–71

Contents lists available at ScienceDirect

Nuclear Instruments and Methods in Physics Research A

journal homepage: www.elsevier.com/locate/nima

Long-term residual radioactivity in an intermediate-energy proton linac

J. Blaha [a], F.P. La Torre [a,b,*], M. Silari [a], J. Vollaire [a]

[a] CERN, 1211 Geneva 23, Switzerland
[b] University of Bern, AEC-LHEP, Sidlerstrasse 5, 3012 Bern, Switzerland

ARTICLE INFO

Article history:
Received 28 November 2013
Received in revised form
3 March 2014
Accepted 29 March 2014
Available online 8 April 2014

Keywords:
Radiation protection
Induced radioactivity
Residual dose
Monte-Carlo
FLUKA
Dump

ABSTRACT

A new 160 MeV H^- linear accelerator (LINAC4) is being installed at CERN to replace the present 50 MeV LINAC2 as proton injector of the PS Booster (PSB). During operation, the accelerator components will be activated by the beam itself and by the secondary radiation field. Detailed Monte Carlo simulations, for various beam energies and several decay times, were performed to predict the residual radioactivity in the main accelerator components and to estimate the residual dose rate inside the tunnel. The results of this study will facilitate future dismantling, handling and storage of the activated parts and consequently minimize the radiation dose to involved workers. The component activation was also compared with the exemption limits given in the current Swiss legislation and to the CERN design values, in order to make predictions for the future storage and disposal of radioactive waste. The airborne radioactivity induced by particles escaping the beam dump and the activation of the beam dump cooling water circuit were also quantified. The aim of this paper is to provide data of sufficiently general interest to be used for similar studies at other intermediate-energy proton accelerator facilities.
© 2015 CERN for the benefit of the Authors. Published by Elsevier B.V. This is an open access article under the CC BY license (http://creativecommons.org/licenses/by/4.0/).

1. Introduction

The estimation of the induced radioactivity in an accelerator facility is particularly important for maintenance interventions and the final disposal of radioactive waste. Safety is the main reason to perform a radiation protection study already during the design and construction phase. It must be demonstrated that the ALARA (As Low As Reasonable Achievable) principle has been taken into account in the design of the new facility. Components that could be activated must be designed in such a way as to facilitate their dismantling, handling and storage in order to minimize the radiation dose to workers.

LINAC4 is a new 160 MeV H^- accelerator which in a few years will be the source of protons for all accelerators at CERN. It is an 80-m long normal-conducting linac made of an H^- source, a Radio Frequency Quadrupole (RFQ), a chopping line and a sequence of three accelerating structures: a Drift-Tube Linac (DTL), a Cell-Coupled DTL (CCDTL) and a Pi-Mode Structure (PIMS) [1,2]. LINAC4 will operate at 1.1 Hz, with a peak current of 40 mA and a pulse length of 0.4 ms as Proton Synchrotron Booster (PSB) injector. These parameters correspond to 0.08% beam duty cycle and 0.032 mA average current or 2×10^{14} protons/s, equivalent to a beam power of 5.1 kW at the top energy of 160 MeV. LINAC4 has been designed to replace the present 50 MeV LINAC2 as injector of the PSB. The higher injection energy will allow the production by the PSB of beams with increased brightness as required by the High-Luminosity LHC (Large Hadron Collider). LINAC4 accelerating structures have also been designed to be the front-end of a future high-power Superconducting Proton Linac (SPL) [3].

LINAC4 is terminated by a dump collecting the beam which is not intended for further utilisation. When the beam interacts with the dump, hadronic interactions produce mixed radiation fields with large numbers of neutrons and other highly penetrating particles. Moreover, the material of the dump becomes highly activated. In addition, the LINAC4 accelerator complex is built in such a way (e.g. depth and orientation of the tunnels) that it allows a future possible connection to the SPL. Consequently, the dump will not be integrated inside the wall as it is a common solution in similar facilities, but it will be placed at the junction between the accelerator and the transfer tunnel (Fig. 1). Therefore an effective shielding surrounding the dump is needed in order to limit activation of the adjacent structures and to protect the personnel accessing the machine.

Activation of the accelerator components at energy between 3 and 160 MeV generates a large volume of (mostly weakly) radioactive stainless steel and copper, which also include permanent magnetic quadrupoles made of a samarium–cobalt alloy. These

* Corresponding author at: CERN, Route de Meyrin, CH-1211, Geneva 23, Switzerland. Tel.: +41 227677752.
E-mail address: francesco.paolo.la.torre@cern.ch (F.P. La Torre).

http://dx.doi.org/10.1016/j.nima.2014.03.058
0168-9002/© 2015 CERN for the benefit of the Authors. Published by Elsevier B.V. This is an open access article under the CC BY license (http://creativecommons.org/licenses/by/4.0/).

components will be subjected to very different levels of activation, depending on the beam loss patterns, on the type of material and on the geometry.

2. Overview of literature data

Various radiation protection studies for new linear accelerator facilities have been published in recent years. Popova et al. [4,5] calculated the expected residual dose rates for commissioning stages and maintenance work at the US Spallation Neutron Source (SNS) accelerator facility. Ene et al. and Tchelidze and Stovall [6,7] performed a first estimate of the shielding required for the superconducting linear accelerator of the European Spallation Source (ESS). They also provided a preliminary characterisation of the residual radioactivity inside the accelerator tunnel for routine maintenance. Nakashima et al. and Yamamoto [8,9] provided beam loss estimations and dose rate calculations for the radiation shielding design of the Japanese high-intensity proton accelerator project (J-PARC). Ferrari et al. [10] used Monte Carlo simulations for optimising some aspects of the shielding of the MYRRHA proton beam line.

Most of these studies focus on shielding design and operational radiation protection requirements. Ene et al. [6] and Ferrari et al. [10] provide dose rate maps and information on the produced radionuclides, but at much higher energies than the present study. This paper discusses in detail extensive calculations of the residual radioactivity in CERN LINAC4, performed in view of its decommissioning at the end of its operational lifecycle. Dose rates were estimated after 30 years of operation for several cooling times up to 2 years. The induced radioactivity and the full radionuclide inventory were assessed in the main components of the three accelerating sections and in the beam dump, for cooling times ranging between 1 day and 500 years. The estimations of the airborne radioactivity, cooling water activation, committed effective dose for the beam dump are discussed in detail. Complete information on beam loss assumptions, accelerator structures and dump components are also provided.

The aim of this paper is to provide data and guidelines that can be of use for estimating the residual radioactivity (both in terms of dose rates and radionuclide composition) in proton accelerators of similar energies, not necessarily linacs. Apart from linear accelerators used e.g. as injectors to high-energy machines, it should be considered that there is an increasing number of 200–250 MeV proton accelerators being installed in hospitals worldwide for cancer radiation therapy [11,12]. These machines are either synchrotrons or cyclotrons, but proton therapy linacs are also under development [13,14]. The results presented in this paper can easily be scaled by the beam loss rate (number of lost particles per unit time).

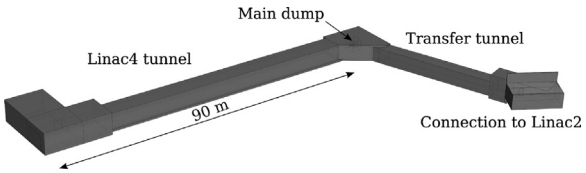

Fig. 1. Layout of the LINAC4 underground tunnel complex.

3. FLUKA calculations

Monte Carlo models used to estimate induced radioactivity in accelerator components must be able to reliably predict nuclide production in arbitrary target elements and for neutron energies ranging from thermal to a value close to the maximum accelerator energy. In this study the Monte Carlo code FLUKA [15,16], which is an appropriate code for estimating induced radioactivity in a wide range of accelerator facilities [17], was used.

Since the statistical uncertainty of the FLUKA simulations on the calculated values is within a few per cent, they are not quoted in tables and figures. The estimation of a systematic error to the hadronic interaction model is very difficult, since there is not always the possibility of comparing predictions to experimental data. The existing data point out that, on average, the agreement of FLUKA predictions of data is at level of about 10% [18].

3.1. Beam loss assumptions and irradiation profile

In a linear accelerator the equipment activation is produced by scattered particles escaping from the fields generated for controlling beam focusing and acceleration and hitting the vacuum chamber. It is hard to predict and identify the beam loss locations because they will not be equally distributed along the machine. Losses typically occur in the aperture restrictions of quadrupoles, due to the possible mismatch between linac sections. According to the estimated particle loss distribution, it was assumed that constant losses of 0.1 W occur every 10 m at selected points along the machine. This value comes from the analysis of the beam losses [19] for a 6% duty cycle scenario, indicating a maximum loss of 1 W in some "hot spots". During the LINAC4 operation as PSB injector at 0.033% duty cycle, losses would be theoretically reduced by a factor of 180 although it is expected that the sensitivity of the beam loss monitors would not allow reaching such a low loss level. A conservative value of 0.1 W per loss location was therefore assumed, 18 times higher than the minimum achievable loss level [20]. Table 1 shows the seven beam losses for the three main accelerating structures with a total length of 70 m. It is evident that with increasing energy the number of lost particles decreases for constant lost beam power. The calculation of the induced radioactivity was performed in three positions (noted in bold in Table 1), representative of typical aperture restrictions in the various sections of LINAC4: the first drift tube of the third DTL tank at 31 MeV, the quadrupole at 80 MeV within the CCDTL section and the last quadrupole at 155 MeV within the PIMS section. For each position the calculations took into account the activation due to the two loss points upstream and downstream of the one under study, a rather innovative approach in this type of study.

The induced radioactivity depends on the irradiation profile, which includes periods of operation at various beam intensities alternating with shutdown (maintenance) periods. Although the LINAC4 irradiation profile during its 30 years of planned operation

Table 1
Beam loss assumptions along the main accelerating structures. The three activation study points are shown in bold.

	DTL		CCDTL		PIMS		
Distance (m)	4	**12**	23	**35**	45	55	**66**
Energy (MeV)	11	**31**	57	**80**	100	128	**155**
Beam loss (p/s)	5.67E+10	**2.01E+10**	1.09E+10	**7.80E+09**	6.24E+09	4.88E+09	**4.03E+09**

Table 2
LINAC4 operation scenarios [21] and corresponding parameters (irradiation time and average intensity) of the irradiation profiles as implemented in FLUKA. One month pause between the commissioning and reliability run, and six months pause between reliability run and normal operation were considered.

	Mean power (W)	**Duration**	**Irradiation time** (s)	**Average intensity** (p/s)	**Total number of protons**
Commissioning run	2841.6	1 month (12 h/day)	2.63E+06	5.54E+13	1.48E+20
Reliability run	710.4	9 months (24 h/day)	2.37E+07	2.77E+13	6.56E+20
Normal operation	2841.6	30 years (2 h/week)	9.47E+08	1.33E+12	1.26E+21

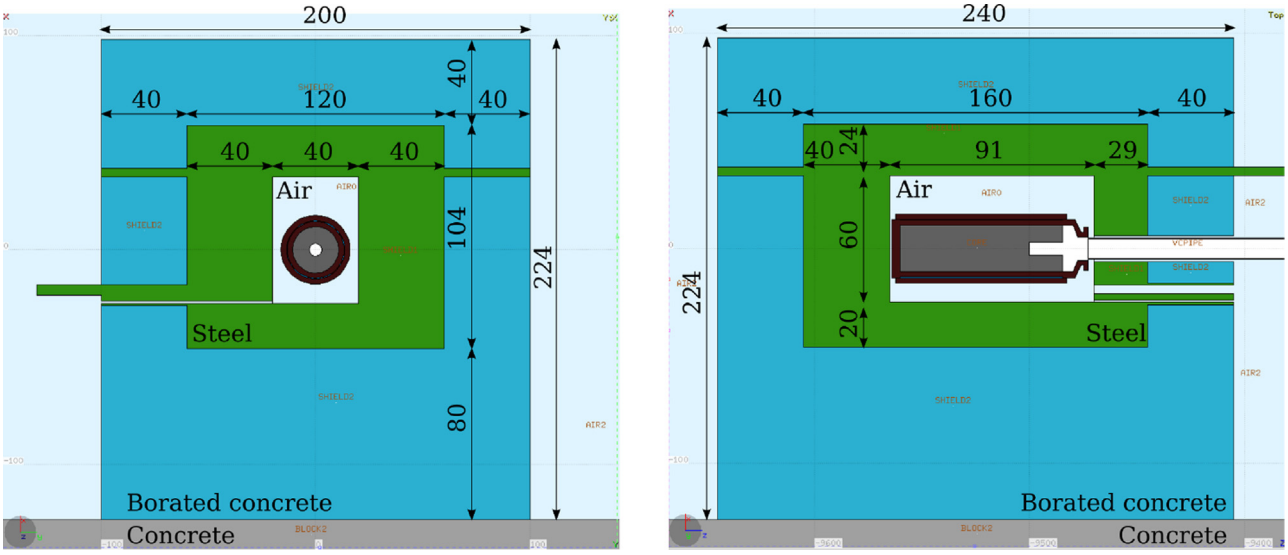

Fig. 2. Front (left) and side (right) views of the beam dump and its shielding as implemented in FLUKA. Dimensions are in centimetres.

is clearly impossible to predict exactly, a simplified but quite realistic irradiation profile was derived from the present LINAC2 yearly schedule, which consists of an average operating time of 5000 h/year. To include a safety margin, an average of 7000 h/year was used in the present calculations (corresponding to the yearly schedule of LINAC2 without the year-long shutdown every 4 years).

Concerning the beam dump activation, three operation periods of LINAC4 were taken into account: the one month commissioning phase with a nominal beam power of 2.84 kW, the nine months reliability run with 1/4 of the nominal power to asses the operational availability of the machine before connection to the PSB, and the normal operation during the LINAC4 life time when the dump will be exposed to the beam only occasionally. More details for each operation phase are listed in Table 2.

3.2. Geometry and material choice

The simulations were performed with FLUKA (version 2011.2.17) using a detailed geometrical model of the main accelerating structures based on the existing geometry implemented a few years ago for a previous study [22,23]. The geometry includes three DTL tanks with permanent magnetic quadrupoles (PMQ) housed in the drift tubes; seven CCDTL modules of three tanks, with PMQs between tanks and electro-magnetic quadrupoles (EMQ) between modules [24]; 12 tanks for the PIMS made of 7-cell pi-mode structures with external EMQs.

The beam dump consists of a core and its shielding. A cylindrical graphite core, with an effective thickness of 60 cm, is surrounded by a stainless steel jacket with incorporated water cooling system [25]. The shielding, which was designed to fulfill both radiation protection requirements and structural constraints, consists of steel blocks surrounding the core and borated concrete blocks used as the outermost layer. The borated concrete was chosen to enhance its shielding properties against neutrons as well as to lower the induced activity in the concrete shielding. Overall dimensions of the shielding are $240 \times 200 \times 224\ \mathrm{cm}^3$ (length × width × height) with a total weight of 36.3 tons. The detailed geometry is shown in Fig. 2.

3.3. Physics settings

The full electromagnetic and hadronic cascades were simulated in the main accelerator components including particles back-scattered from the beam tunnel walls. For an accurate description of all the nuclear processes relevant for isotope production, the evaporation of heavy fragments and the coalescence mechanism were explicitly turned on. Default settings for precision simulations were used. The particle transport threshold was set at 100 keV, except for neutrons that were transported down to thermal energies. The low energy neutron transport (below 20 MeV) was performed using the multi-group approach, updated to the new 260 group library. The decays option was used to simulate radioactive decays and to set the corresponding transport conditions. This allows the time evolution of induced radioactivity to be calculated analytically for fixed cooling times, considering daughter nuclei as well as the associated radiation.

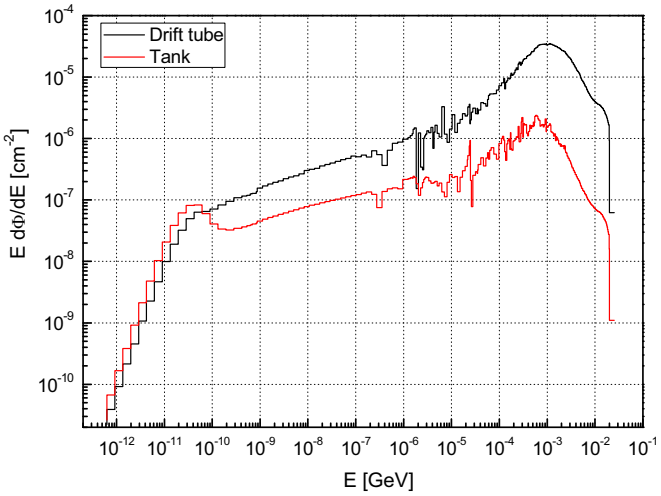

Fig. 3. Comparison of the neutron fluence spectra in the first drift tube and in the third tank of the DTL section.

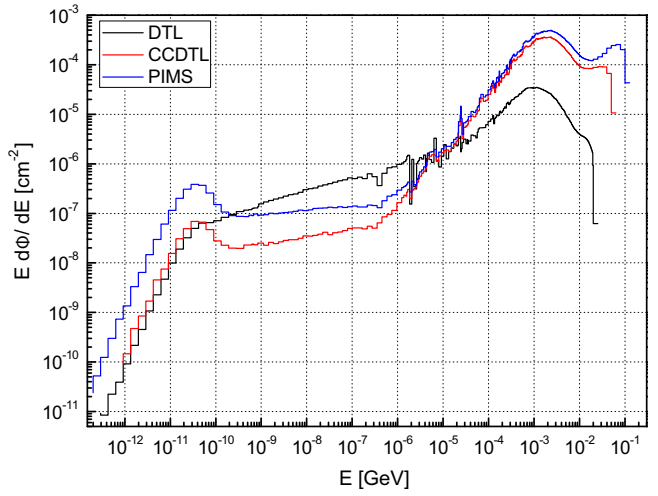

Fig. 4. Comparison of the neutron fluence spectra at the three beam impact points: 31 MeV (DTL), 80 MeV (CCDTL), 155 MeV (PIMS).

3.4. Neutron fluence spectra

Apart for components directly hit by the beam (e.g. collimators or aperture restrictions), most of the induced radioactivity in proton accelerators in the 100 MeV range is due to the stray neutron field. Fig. 3 compares the neutron fluence spectra in the drift tube and in the tank surrounding the beam impact point in the DTL. Fig. 4 compares the neutron energy spectra at the location of the three loss points under study for all sections.

The neutron fluence spectra computed for the beam dump are plotted in Fig. 5 and show that the combination of the iron and borated concrete reduces considerably the secondary neutrons by two orders of magnitude over the whole energy range. The iron layer has significant impact on the high energy neutron component whilst the concrete is more effective from the fast down to the thermal energies.

4. Dose rates

The personnel accessing of the accelerator tunnel after the beam stop, e.g for performing the maintenance of the accelerator elements, will be exposed to remnant radiation originating from the activated part of the machine. In order to estimate the time

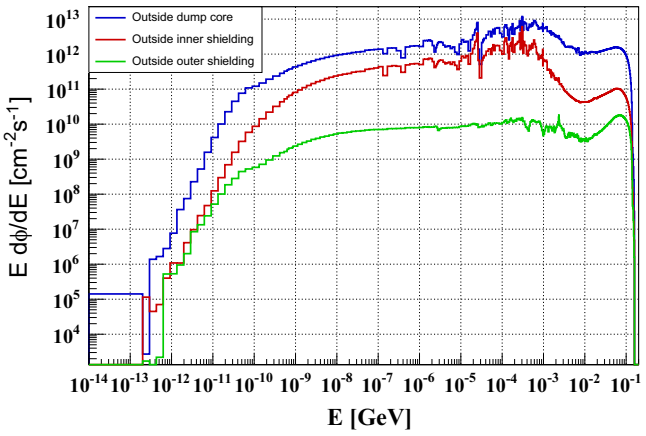

Fig. 5. Neutron fluence spectra at the boundary between dump (air volume around the dump) and inner shielding (steel), between inner and outer shielding (borated concrete), and outside the shielding.

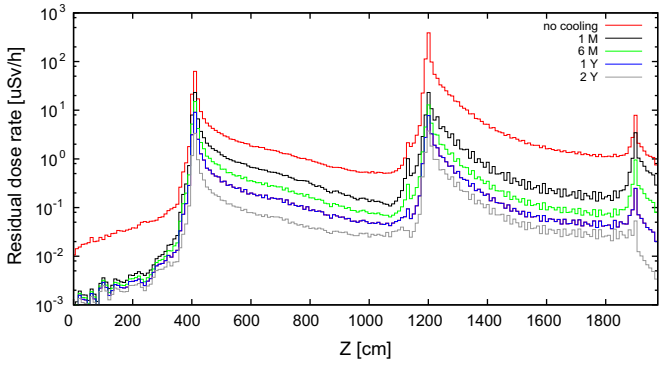

Fig. 6. Ambient dose equivalent rate inside the DTL tank along the beam axis (z) for five decay times.

after which access can be granted, the residual dose rate profiles and maps were calculated for several cooling times. Each plot shown below takes into account the dose rate due to the beam loss point under study and the two loss points downstream and upstream. The ambient dose equivalent rate around the dump was also calculated.

4.1. Dose rates profiles and maps

In the DTL section the dose rates are rather low due to the comparatively low beam energy. Fig. 6 shows the dose rate inside the DTL tank for 5 decay times. Dose rate peaks of about 100 μSv/h and 500 μSv/h can be observed at the beam impact points at 11 MeV and 31 MeV, respectively. The last peak is due to the dose rate from the downstream loss point at 57 MeV energy.

Whereas the DTL quadrupoles are shielded by the drift tube and by the tank, the quadrupoles in the other sections of the accelerator are directly accessible. The ambient dose equivalent rate inside the CCDTL tank is shown in Fig. 7. A dose rate of almost 10 mSv/h can be reached at the 80 MeV beam loss point, which is a critical location because of the permanent magnetic quadrupole (PMQ) near the vacuum chamber. A few localized hot spots in correspondence of the quadrupoles can push the dose rate up to 100 μSv/h at 10 cm from the tank. On the other hand, the dose rate decreases quickly far from the beam loss points reaching 0.1 μSv/h in just 1 month of cooling time. The difference in the dose rate between the first (EMQ) and the second (PMQ) activation point is rather due to the different material compositions than the difference in energy. Starting from 6 months of cooling time the

dose rate peaks caused by the PMQ magnets along the CCDTL section are clearly visible. In the PIMS structure the dose rate distribution is more uniform (Fig. 8). Although the beam losses can occur at the maximum energy, the highest dose rate does not exceed 2 mSv/h.

The dose rate profiles in the dump proximity are shown in Fig. 9: the ambient dose equivalent rate falls down steadily due to fast decaying nuclei in activated parts of the shielding. In concrete it is mainly because of the relatively short half life ($T_{1/2} = 15$ h) of ^{24}Na. The dose rate reaches a level of a few μSv/h at 1 m distance after 1 day of cooling. After about one week the residual dose rate remains almost stable and decreases slowly as the long lived ^{22}Na ($T_{1/2} = 2.6$ years) in concrete decays. The highest values of the residual dose rate outside the dump shielding are in upstream locations (for $Z > -9400$ cm in Fig. 9 right) because of the activated beam pipe and due to the residual radiation coming from openings in the shielding around the pipe and holes for dump services.

The dose rate maps in Figs. 10 and 11 were calculated along the z-axis of the accelerator (top view, y-axis). Fig. 10 shows the dose rate plots in the PIMS section for three beam losses (100 MeV, 128 MeV and 155 MeV) and several cooling times (1 month, 6 months, 1 year and 2 years). In Fig. 11 the maps providing the spatial distribution of ambient dose equivalent rates around the dump are shown for different cooling times ranging from 1 h to 2 years.

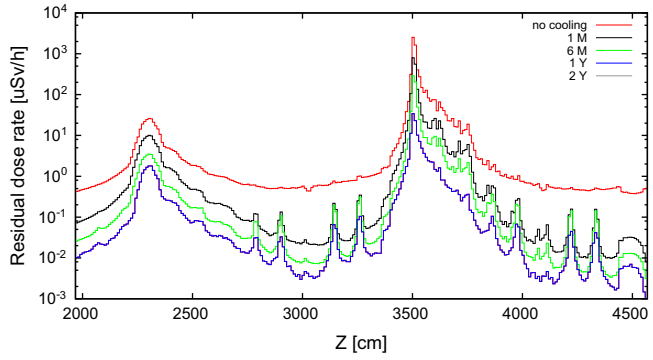

Fig. 7. Ambient dose equivalent rate inside the CCDTL tank along the beam axis (z) for five decay times.

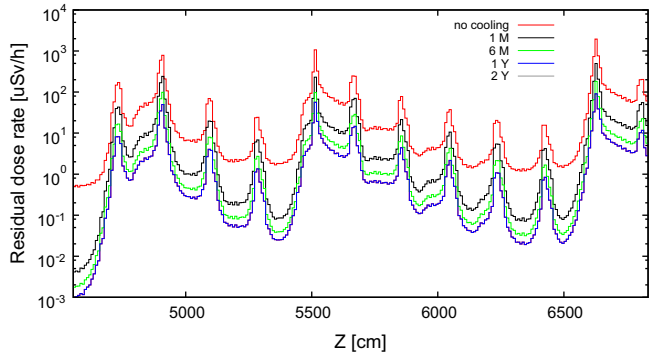

Fig. 8. Ambient dose equivalent rate inside the PIMS tank along the beam axis (z) for five decay times.

5. Induced radioactivity

The residual radioactivity for the most important accelerator components was calculated for several decay times. Not only the activation produced by the direct impact of the beam at the given loss point was estimated, but also the induced radioactivity due to the secondary particles coming from the two loss points downstream and upstream. The induced specific activity A_i for each radionuclide i and for several cooling times was compared with the CERN exemption values LE_i used in design studies for future accelerators [26]. These values represent, for each nuclide, the minimum of the exemption limits that are likely to be adopted by future European Directives and national legislations and are thus considered as conservative values. They are much more restrictive than those provided e.g. in the present Swiss legislation [27] as shown in Table 3. Thus, for a mixture of n radionuclides a ratio R is defined using the summation rule:

$$R = \sum_{i=1}^{n} \frac{A_i}{LE_i} \quad (1)$$

where both A_i and LE_i are expressed in Bq/kg.

5.1. Specific activity in linac components

In the DTL section, the proton beam impinges on the first drift tube of the third tank. The specific activity was estimated in the following components of the third tank: the drift tubes; the permanent magnetic quadrupoles (PMQ); the stems; the girders; the tank; the vacuum chamber and the electromagnetic quadrupole (EMQ) upstream of the loss point; the waveguide and the support closest to the loss point. Fig. 12 shows the specific radioactivity as a function of cooling time for the DTL. It is interesting to notice that the PMQs are the most active components, as expected due to their high cobalt content. After 2 years of

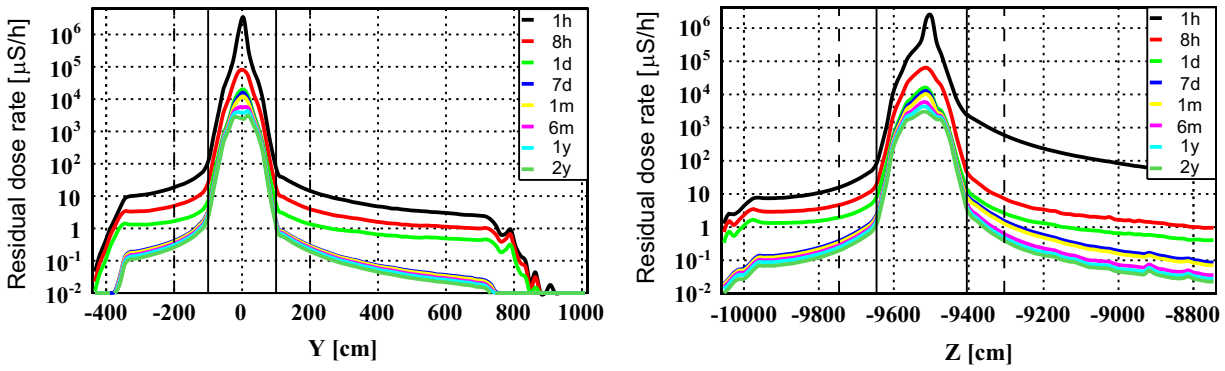

Fig. 9. Ambient dose equivalent rates after several cooling times on an imaginary plane at the center of the dump perpendicular (left) and along the beam direction (right) after 30 years of LINAC4 operation. Full vertical lines indicate the shielding boundary and dashed lines mark a 1 m distance from the shielding.

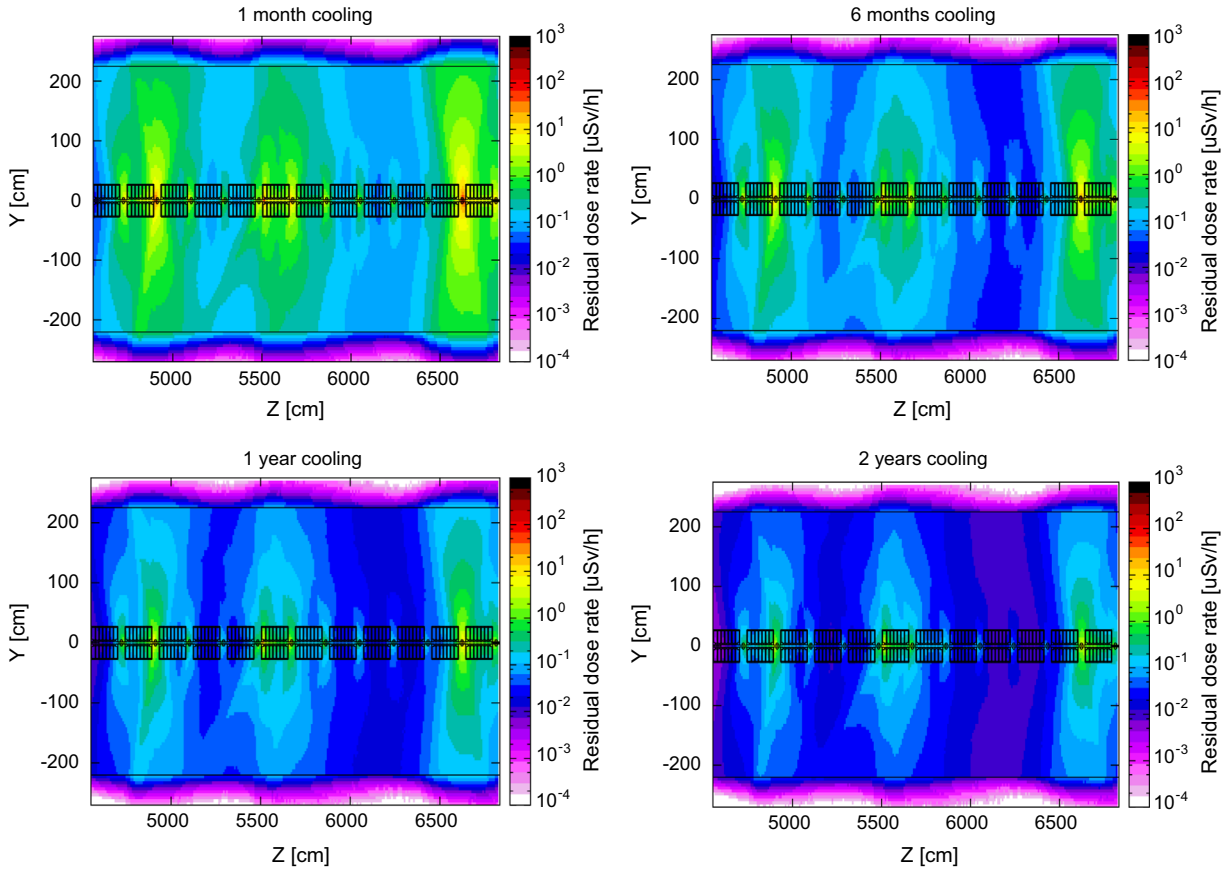

Fig. 10. Ambient dose equivalent rates calculated in the PIMS section for several cooling times after 30 years of LINAC4 operation.

decay time, the main contributors to R in the PMQs are ^{60}Co (57%) and ^{152}Eu (26%), whereas ^{55}Fe (which has a much higher LE) mostly contributes to the total activity (69%). For the drift tubes almost all activity (and R) is due to ^{65}Zn and ^{60}Co, but the long decay time is due to ^{63}Ni, which is the longest-lived radionuclide ($T_{1/2} = 96$ years) found in the radionuclide inventory. In the CCDTL section the proton beam impinges on the vacuum chamber between the first and the second tank of the 5th module. The specific activity was estimated in the following components: the vacuum chamber and the PMQ between the first and the second cavity; the EMQ closest to the loss point; the tank wall, the copper plating, the first nose-cone, the first drift tube, the copper and stainless steel stem downstream of the loss point; the waveguide and the support closest to the loss point. The most active component in the CCDTL is the vacuum chamber because it is directly hit by the beam (Fig. 13). After 2 years of cooling, the major contribution to the activity comes from ^{55}Fe (76%) and ^{54}Mn (9%), but the ratio R is dominated by ^{54}Mn (90%) and ^{57}Co (4%). ^{44}Ti/^{44}Sc and ^{63}Ni are responsible for the residual radioactivity at very long decay times. In the PIMS section the proton beam impinges on the vacuum chamber between the 11th and the 12th tank. The residual radioactivity was estimated in the following components: the vacuum chamber between the 11th and the 12th tank; the EMQ adjacent to the vacuum chamber; the left wall and the external wall of the 12th tank downstream of the loss point; the external wall of the 11th tank upstream of the loss point; the nose-cone and the copper cylinder of the 12th tank located downstream of the loss point; the support and the waveguide closest to the loss point. As evident from Fig. 14, the most active components are the vacuum chamber and the EMQ, with specific activity higher than 1x10^7 Bq/kg after 1 year of cooling. For the vacuum chamber, the major contribution to R after 2 years of cooling comes from ^{54}Mn (90%) and ^{57}Co (4%), whereas the major contribution to the activity comes from ^{55}Fe (65%) and ^{49}V (10%). The EMQs activity is dominated by ^{55}Fe (79%) and ^{54}Mn (11%), but the main contribution to R is due to ^{54}Mn (92%) and ^{60}Co (3%). Table 4 shows the fraction R of CERN design exemption limits for some selected components after 2 years of cooling time.

5.2. Specific activity in dump components

Assuming 2 years of cooling time after 30 years of accelerator operation, mainly long lived radionuclides remain in the dump materials. In case of the dump core, which consists of pure carbon, almost all total activity and R are due to ^{3}H. For other parts of the core made of stainless steel, the main contributors are ^{55}Fe (76%) and ^{54}Mn (11%), contrary to R where the main contributors are ^{54}Mn (88%) and ^{60}Co (7%). A different situation is found for the steel shielding where ^{55}Fe (49%) and ^{60}Co (38%) account for most of the activity. The low LE_i value associated with ^{60}Co leads to its 86% contribution to R. The second most important contributor to R is ^{54}Mn (11%). The difference in the values for the steel of the dump core and of the shielding is due to their different material compositions. In case of the borated concrete shielding, the principal contributions to the activity come from ^{3}H (75%) and ^{55}Fe (11%). As expected, the contribution to R is dominated by ^{22}Na (87%); the second significant contribution is from ^{54}Mn (11%). Finally, the specific activity and fraction of the exemption limits for each component during the dump decommissioning are summarized in Table 5.

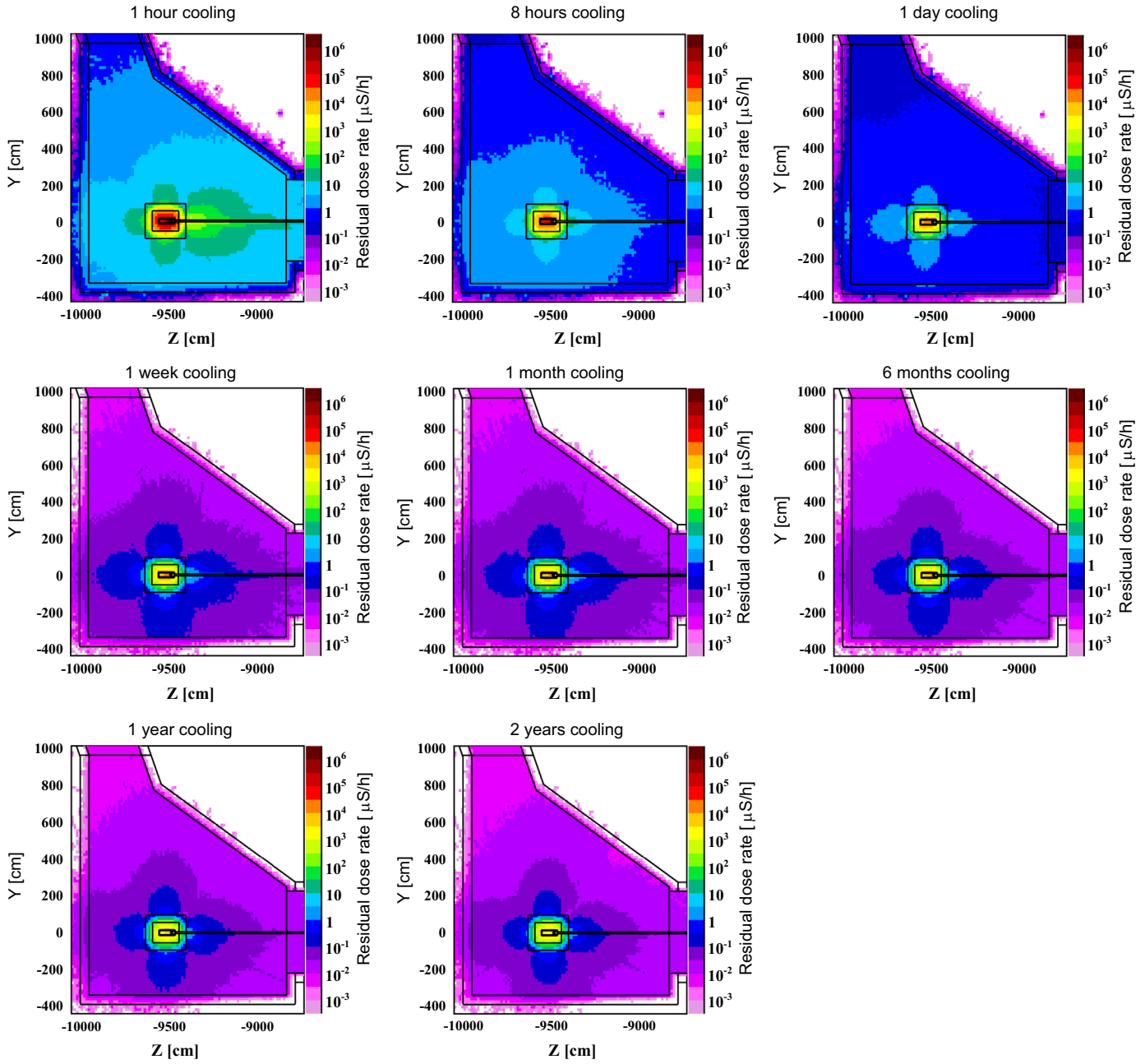

Fig. 11. Ambient dose equivalent rates calculated in the dump section for several cooling times after 30 years of LINAC4 operation.

5.3. *Total radioactivity distribution in linac components*

In order to evaluate the activity distribution inside the Linac a region-independent scoring (Cartesian binning) of the total radioactivity over the three beam loss points in each section of the linac was carried out for 5 cooling times: immediately after the end of the operation and after 1 month, 6 months, 1 year and 2 years. Fig. 15 shows the activation profile of the fifth CCDTL module, which consists of three tanks. The beam loss points at 35 m distance and 80 MeV energy are clearly visible.

6. Airborne radioactivity and water activation

Personnel accessing of the LINAC4 tunnel shortly after the beam is stopped can be exposed not only to residual radiation from the activated structures, but also to radiation from the activated air through external exposure and inhalation. Moreover, certain amount of airborne radioactivity will be released off-site of the building. It is therefore necessary to estimate the air activation and its radiological impact. Since the main contribution to the airborne radioactivity and water activation will come from the dump only this component was considered for this study.

6.1. *Residual and released air activity*

The time evolution of the activity was calculated for all radionuclides produced in the air by folding the track-length spectra computed by FLUKA for different hadrons (n, p, π^+, π^-) with the energy dependent production cross-section of the target nuclide in the air compound. This two-step technique [28] allows obtaining the production yields with sufficient statistical precision also for low-density media in comparison of computing the same

Table 3
Main radionuclides found in the LINAC4 components and current (Swiss) and future (design) exemption limits.

Nuclide	$T_{1/2}$	LE (Bq/kg)	
		Swiss [27]	Design [26]
^{3}H	12.3 years	2.00E+005	1.00E+005
^{22}Na	2.6 years	3.00E+003	1.00E+002
^{44}Ti/Sc	47.3 years	2.00E+003	2.00E+003
^{45}Ca	163 days	1.00E+004	1.00E+004
^{46}Sc	83.83 days	7.00E+003	1.00E+002
^{48}V	16.24 days	5.00E+003	1.00E+003
^{49}V	330 days	6.00E+005	6.00E+005
^{51}Cr	27.7 days	3.00E+005	1.00E+005
^{52}Mn	5.6 days	6.00E+003	1.00E+003
^{54}Mn	312.5 days	1.00E+004	1.00E+002
^{55}Fe	2.7 years	3.00E+004	3.00E+004
^{56}Co	78.76 days	4.00E+003	1.00E+002
^{57}Co	270.9 days	5.00E+004	1.00E+003
^{58}Co	70.8 days	1.00E+004	1.00E+003
^{59}Fe	44.5 days	6.00E+003	1.00E+003
^{60}Co	5.27 years	1.00E+003	1.00E+002
^{63}Ni	96 years	7.00E+004	7.00E+004
^{65}Zn	243.9 days	3.00E+003	1.00E+002
^{88}Y	106.6 days	8.00E+003	8.00E+003
^{88}Zr	83.4 days	3.00E+004	3.00E+004
^{145}Sm	340 days	5.00E+004	5.00E+004
^{149}Eu	93.1 days	1.00E+005	1.00E+005
^{152}Eu	13.33 years	7.00E+003	1.00E+002
^{154}Eu	8.8 years	5.00E+003	1.00E+002
^{155}Eu	4.96 years	3.00E+004	1.00E+003

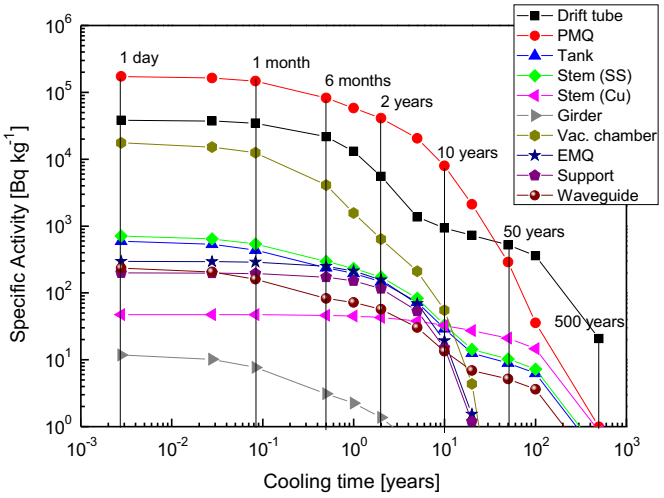

Fig. 12. Specific radioactivity as a function of cooling time in the main DTL components.

quantity in FLUKA directly. The total yield for each radionuclide is given in Table 6.

Assuming a simple laminar flow model with a partial air exchange of $Q = 2000\ \mathrm{m^3/h}$ out of a total air volume $V = 1330\ \mathrm{m^3}$ of the tunnel, one can calculate the activity of a radionuclide at the end of the irradiation time t_{irr} for a given beam intensity I by [29]

$$A_{res} = \frac{Y\lambda I}{\lambda'}(1 - e^{-\lambda' t_{irr}}) \quad \text{where } \lambda' = \lambda + \frac{Q}{V}.$$

Y and λ denote the radionuclide production yield per primary proton and the decay probability per unit time, respectively. λ' is the effective decay constant taking into account the air exchange during the irradiation (the ratio Q/V represents the fraction of the total air renewed per unit time). The saturation activity, i.e. the activity at the equilibrium between radionuclide production and decay including the

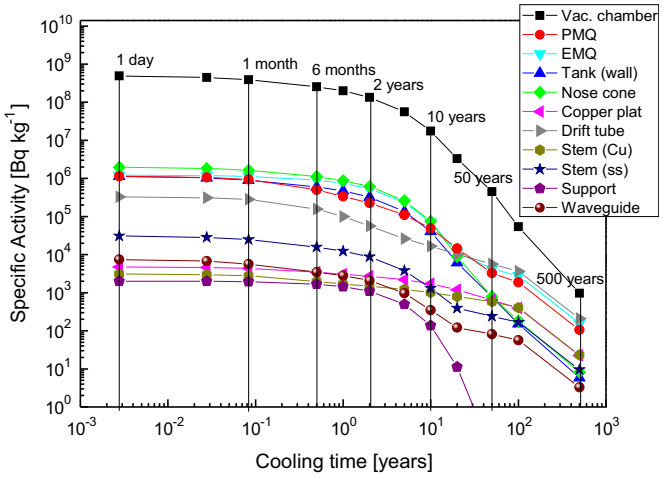

Fig. 13. Specific radioactivity as a function of cooling time in the main CCDTL components.

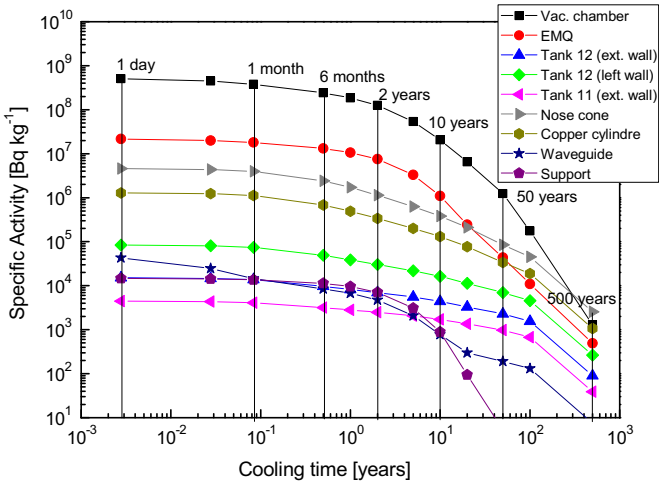

Fig. 14. Specific radioactivity as a function of cooling time in the main PIMS components.

air renewal, is reached after about 90 min. The total residual activity just after the beam stop has been estimated to be about 33 MBq. The contribution of each radionuclide to the total activity is listed in Table 6.

The activity released into the atmosphere during the irradiation can be obtained for each radionuclide by [29]

$$A_{atm} = \frac{Y\lambda I}{\lambda'}\frac{Q}{V}\left(t_{irr} - \frac{1 - e^{-\lambda' t_{irr}}}{\lambda'}\right)e^{-\lambda t_{rel}},$$

where t_{rel} is the time needed for the activated air to reach the release point. Its value was estimated, based on the length of the air path and the velocity of the air in the tunnel and in ventilation ducts, to be around 5 min. The annual activity released in the environment during the LINAC4 normal operation phase is about 3 GBq.

6.2. Estimation of committed effective doses

The activity concentrations were calculated with the assumption that the activity in air is distributed homogeneously throughout the LINAC4 tunnel and the dump area, which leads to a value of 25 kBq/m^3. The radiological importance of a radionuclide can be obtained from a comparison of the computed activity

Table 4
Fraction of CERN design exemption limits $R=\sum_i A_i/LE_i$ for the main accelerator components after 2 years of cooling time. All results have a statistical uncertainty lower than 2%.

Component	Material	DTL	CCDTL	PIMS
Vacuum chamber	Stainless steel (316L)	1.67E+00	1.35E+05	1.28E+05
Drift tube	Copper	4.53E+01	2.24E+02	/
PMQ	Samarium–cobalt alloy	9.23E+01	8.62E+02	/
EMQ	Low carbon magnetic steel	1.17E−01	5.95E+02	8.73E+03
Stem	Copper	1.36E−01	5.55E+00	/
Stem	Stainless steel (316L)	8.79E−02	8.87E+00	/
Tank	Stainless steel (304L)/Copper (PIMS)	8.59E−02	1.91E+01	9.58E+01
Girder	Aluminium (AW6082)	3.24E−03	/	/
Nose-cone	Stainless steel (304L)/ Copper (PIMS)	/	6.17E+02	2.47E+03
Cylinder	Copper	/	/	8.30E+02
Plating	Copper	/	6.20E+00	/
Waveguide	Stainless steel (304L)	5.13E−03	1.60E+00	6.62E+00
Support	Steel (ST-37)	2.42E−02	4.68E−01	5.53E+00

Table 5
Specific activity and fraction of CERN design exemption limits for the dump after 30 years of operation and 2 years of cooling time. All results have a statistical uncertainty lower than 1%.

Component	Material	Mass (tons)	Activity (Bq/kg)	$\sum_i A_i/LE_i$
Dump core	Graphite/steel	0.34	3.60E+08	4.58E+04
Inner shielding	Steel	15.89	8.72E+05	3.89E+03
Outer shielding	Borated concrete	20.07	2.31E+03	2.17E+00

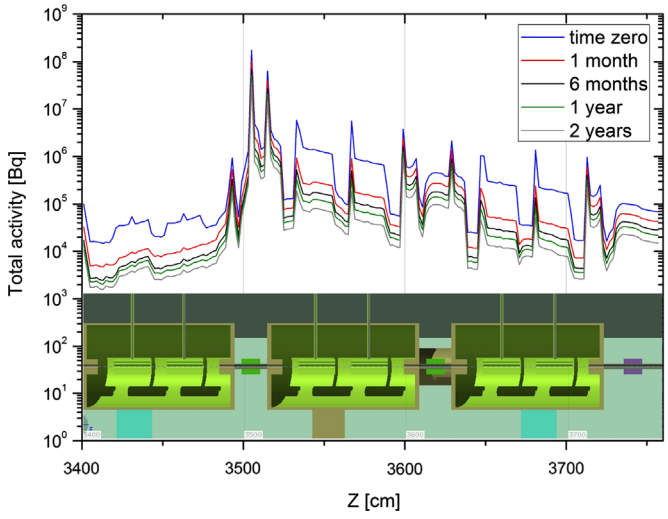

Fig. 15. Profile of the total radioactivity in the 5th CCDTL module along the beam axis (z) for five decay times.

concentration for each radionuclide with the guideline values CA [Bq/m^3][1] for airborne activity concentration according to the Swiss legislation [27]. As shown in Table 6 the most important radionuclides are ^{11}C ($T_{1/2}=20.4$ min), ^{13}N ($T_{1/2}=9.97$ min), ^{15}O ($T_{1/2}=122$ s), and ^{41}Ar ($T_{1/2}=109.34$ min). Those positron emitters account for almost 99% or 97.8% of the total CA or specific activity fractions, respectively.

A worker performing an intervention just after the machine shutdown will be exposed to the external (via immersion in activated air) as well as to internal (via intake of radioactive air through breathing) radioactivity. The effective dose rates due to the external exposure were estimated for a given radionuclide from the fraction of its CA value. The effective dose rates for internal exposure were calculated supposing a standard breathing rate of 1.2 m^3/h and using the dose coefficients for inhalation e_{inh} Sv/Bq as given by the Swiss legislation [27]. The effective dose rates for external exposure were calculated by using the CA values. The total effective dose rate for external exposure and inhalation was estimated to be 3.6 μSv/h. This value is mostly due to external exposure, mainly by the above-mentioned positron emitters.

6.3. Activation of cooling water

The main dump will be connected to a closed demineralised water circuit which is used to cool the main dump, the dumps in the measurement lines and other equipment installed inside the transfer tunnel. The water flowing through the dump cooling system will be activated via hadronic interactions of the secondary particles produced in the dump. In order to estimate the activity of the water flowing inside the dump, the production yields of the radionuclides in the water circuit were calculated. The values obtained for a total irradiated volume of 2.5 l inside the dump are given in Table 7. Then the activity in the cooling water at the end of the irradiation period t_{irr} for a given production rate $P=Y\times I$, where Y is the yield and I is the beam intensity, is calculated by

$$A_1 = P_1(1-e^{-\lambda t_{irr1}}),$$
$$A_2 = P_2(1-e^{-\lambda t_{irr2}})+A_1 e^{-\lambda(t_{offA}+t_{irr2})},$$
$$A_3 = P_3(1-e^{-\lambda t_{irr3}})+A_2 e^{-\lambda(t_{offB}+t_{irr3})},$$

where t_{offA} and t_{offB} stand for the first and the second pause (1 and 6 months) between accelerator operation, respectively; index 1, 2, and 3 corresponds to the commissioning, reliability run and normal operation, respectively. Considering that the cooling loop is closed, one can obtain the activity concentration in Bq/m^3 by dividing the activity by the total volume of cooling water that is estimated to be approximately 1.5 m^3. The results obtained are summarized in Table 7. From a radiological point of view, the most important radionuclides are the long lived ^{3}H and ^{7}Be having a total activity at the end of the LINAC4 life time equal to about 7.8 and 1.8 MBq, respectively. It should be noted that ^{3}H will be distributed homogeneously along the whole cooling loop with an activity concentration increasing proportionally with the irradiation time up to about 5.2 Bq/cm^3 at the end of the accelerator life time. On the other hand, ^{7}Be will be captured by a special filter (e. g. in demineraliser) and thus it will increase the activity in those parts of the loop.

Table 7 compares the total and specific activity with the exemption limits as given by the Swiss legislation [27]. This legislation is

[1] The CA is a guidance value for chronic occupational exposure to airborne activity. Exposure to an airborne activity concentration CA for 40 h/week and 50 weeks/year yields a committed effective dose of 20 mSv [27].

Table 6
Total radionuclide production yields in the air for a proton interaction in the dump and corresponding residual activity and activity released into the atmosphere, airborne activity concentration values (CA) according to the Swiss legislation [27], and dose rates for internal and external exposure of personnel accessing the LINAC4 tunnel. All results have a statistical uncertainty lower than 1%.

Nuclide	Half life (*s*)	Yield per primary	Residual activity (Bq)	Activity released into atmosphere (Bq)	CA (Bq/m^3)	Activity concentration/CA	Dose rate for internal and external exposure (μSv/h)
^{11}C	1.22E+03	5.94E−08	3.72E+06	1.52E+10	7.00E+04	4.00E−02	1.07E−02
^{13}N	5.98E+02	2.26E−07	1.81E+07	6.17E+10	7.00E+04	1.94E−01	1.94E+00
^{15}O	1.22E+02	9.66E−08	9.79E+06	8.64E+09	7.00E+04	1.05E−01	1.05E+00
^{32}P	1.23E+06	3.86E−10	5.35E+01	2.72E+05	2.00E+03	2.02E−05	1.40E−04
^{38}Cl	2.23E+03	3.14E−09	1.45E+05	6.41E+08	4.00E+04	2.72E−03	9.55E−03
^{39}Cl	3.34E+03	5.19E−09	1.85E+05	8.52E+08	2.00E+05	6.98E−04	1.27E−02
^{41}Ar	6.58E+03	3.89E−08	8.32E+05	3.99E+09	5.00E+04	1.25E−02	1.25E−01
Total	–	–	**3.31E+07**	**9.13E+10**	–	**3.56E−01**	**3.15E+00**

Table 7
Total radionuclide production yields in the water cooling circuit for an irradiated volume of 2.5 l for a proton interaction in the dump and corresponding total and specific activity. The latter is calculated assuming a total volume of 1.5 m^3 of water inside the cooling loop. Total activity A_i and activity concentration a_i in water cooling circuit compared to an exemption limit LE_i for a given radionuclide and its relative contribution. All results have a statistical uncertainty lower than 1%.

Nuclide	Half-life	Yield per primary	Total activity (Bq)	Activity concentration (Bq/cm^3)	LE_i (Bq/kg) or (Bq)	$a_i/(LE_i/100)$	$A_i/(100LE_i)$
^{3}H	12.33 years	6.01E−06	7.80E+06	5.20E+00	6.00E+05	8.66E−01	8.66E−05
^{7}Be	53.22 days	1.32E−06	1.76E+06	1.17E+00	4.00E+05	2.93E−01	2.93E−05
Total	–	–	**9.56E+06**	**6.37E+00**	–	**1.16E+00**	**1.16E−04**

applicable (i.e. the water is considered as radioactive) if the specific activity exceeds one per cent of the exemption limit LE as a weekly mean and/or the total activity release per month is larger than 100 times the LE. It should be stressed that the LINAC4 water cooling circuit is a closed loop and no release of the activated water into the environment is foreseen during its life time.

7. Individual and collective doses for the dump exchange

During LINAC4 operation the dump components as well as its shielding will be highly activated and the residual dose rates will reach levels at which any maintenance or intervention must be planned in advance. The worst case is the loss of the dump functionality that will result in its complete replacement. In order to protect personnel who will perform such an intervention, the procedure must be optimized based on the ALARA (As Low As Reasonably Achievable) principle. For this reason the dump shielding was designed in a way that it permits an easy access to the core and its removal.

Individual and collective doses received by workers who will be involved in the dump exchange were calculated for each intervention step knowing the detail work procedure including the number of workers, their precise locations and duration of each work action. The residual dose rates at a given location and estimated individual and collective doses for different cooling times are summarized in Table 8. The individual and collective doses are less than 0.2 mSv if 8 h of cooling time are considered. Those values are well under the CERN design criteria and therefore the established intervention scenario can be considered as optimized.

Table 8
Expected maximum individual and collective doses for the dump exchange intervention, and maximum dose equivalent rate during the intervention.

Cooling time	1 h	8 h	1 day	1 week	1 month
Individual dose (μSv)	1585	126	23	15	12
Collective dose (μSv)	2055	167	32	20	16
Dose rate (μSv/h)	698	57	10	7	6

8. Results and conclusions

A set of FLUKA simulations using a detailed geometrical model of the accelerator was carried out to predict the induced radioactivity in LINAC4 after several years of operation and for various decay times. The following estimations were performed: residual radioactivity in the main components; comparison with the future (design) exemption limits; profile of the total activity for the three beam loss points under study; dose rate in the whole accelerator structure for relevant cooling times.

It is predicted that most of the components in the DTL can be dismantled soon after the final shutdown. The mean storage time required is 2 years for the vacuum chamber and 10 years for the drift tubes. The PMQs will exceed the limits for at least 50 years after final shutdown. In the CCDTL the dismantling is recommended after 2 years of cooling. After 10 years about half of the accelerator components are below the limits. The longest decay time foreseen is 100 years for the vacuum chamber. In the PIMS the dismantling should start after 5 years of cooling. Half of the PIMS components are expected to be below the limits after 20 years. The longest estimated decay time is 100 years for the vacuum chamber.

Dose rates at 10 cm from the tank vary in the range of 0.1–1 μSv/h for the DTL and between 1 μSv/h and 100 μSv/h for the CCDTL. Although the beam losses can occur at the maximum energy in the PIMS, the highest dose rate does not exceed 100 μSv/h at 10 cm from the tank.

The residual dose rates show that the dump area will be accessible after a short cooling time. The activity released into the atmosphere was estimated and the effective dose due to airborne radioactivity was found to be under the limits for workers accessing the tunnel. Radionuclide production in water was quantified for the dump cooling system. The individual and collective doses for the dump exchange were calculated. The

intervention for the dump replacement is possible within 24 h after a dump failure. The radionuclide inventory for all dump materials was established and give an important input for radioactive waste management during the decommission of the LINAC4.

It is important to point out that the values of the induced radioactivity predicted in this study were estimated for the most probable scenario at the present time, i.e. 0.1 W of beam losses every 10 m for 30 years of irradiation. In case of different losses, irradiation profile or machine operating parameters, an increase/decrease in beam losses can be expected and, therefore, in machine activation depending on the new scenario. It is most likely that the activation will not be uniformly distributed along the machine. The components indicated as activated in this study could in reality be only partially radioactive, depending on the distance from the beam loss points. It may be feasible that a given component is cut in pieces, and each piece is either disposed as conventional waste or stored as radioactive. This is of course hard to predict at this stage and only operational radiation protection measurements on each machine components after the final shutdown will provide the real activation scenario and allow deciding e.g. on the required cooling time.

Acknowledgements

The authors are grateful to Maurizio Vretenar for providing the technical specifications needed for the present study and for many useful discussions.

References

[1] M. Vretenar, et al., LINAC4 Technical Design Report, Technical Report CERN-AB-2006-084, CARE-Note-2006-022-HIPPI, CERN, Geneva, December 2006.
[2] M. Vretenar, et al., The LINAC4 Project at CERN (CERN-ATS-2011-041), 2011, 4 p.
[3] M. Vretenar, et al., Conceptual Design of the SPL II: A High-Power Superconducting H^- Linac at CERN, CERN, Geneva, 2006.
[4] I. Popova, J. Galambos, P. Ferguson, F. Gallmeier, Residual dose rate analyses for the SNS accelerator, in: Proceedings of Hadron Beam 2008, HS-2008, 25–29 August, Nashville, Tennessee, USA, 2008, pp. 371–374.
[5] I. Popova, D. Gregory, F. Gallmeier, P. Gonzalez, Radiation measurements vs. predictions the SNS linac commissioning, in: Proceedings of EPAC'06 European Particle Accelerator Conference, 26–30 June 2006, Edinburgh, Scotland, 2006, pp. 977–979.
[6] D. Ene, M. Brandin, M. Eshraqi, M. Lindroos, S. Peggs, H. Hahn, Progress in Nuclear Science and Technology 2 (2011) 382.
[7] L. Tchelidze, J. Stovall, Estimation of Residual Dose Rates and Beam Loss Limits in the ESS Linac, Technical Report ESS/AD/0039, ESS, April 2012.
[8] H. Nakashima, et al., Radiation Protection Dosimetry 115 (2005) 564.
[9] K. Yamamoto, Beam loss and residual dose rate at 100 KW user operation in the J-PARC accelerator, in: Proceedings of Hadron Beam 2010, HS-2010, 27 September–1 October 2010, Morschach, Switzerland, 2010, pp. 400–404.
[10] A. Ferrari, J. Biarrotte, L. Perrot, H. Saugnac, D. VandePlassche, Shielding and activation studies for the design of the MYRRHA proton beamline, in: Proceedings of Shielding Aspects of Accelerators, Targets and Irradiation Facilities, SATIF-11, 11–13 September 2012, Tsukuba, Japan, 2012, pp. 13–27.
[11] Particle Therapy Co-Operative Group ⟨http://ptcog.web.psi.ch/⟩.
[12] U. Amaldi, et al., Nuclear Instruments and Methods in Physics Research Section A 620 (2010) 563.
[13] C. Ronsivalle, et al., The European Physical Journal Plus 126 (2011) 68.
[14] A. Degiovanni, et al., Design of fast-cycling high-gradient rotating linac for protontherapy, in: Proceedings of the 4th International Particle Accelerator Conference, IPAC13, 12–17 May 2013, Shanghai, China, 2013, pp. 3642–3644.
[15] G. Battistoni, S. Muraro, P.R. Sala, F. Cerutti, A. Ferrari, S. Roesler, A. Fasso', J. Ranft, AIP Conference Proceedings 896 (2007) 31.
[16] A. Ferrari, P.R. Sala, A. Fasso', J. Ranft, FLUKA: A Multi-Particle Transport Code, CERN-2005-10, 2005; INFN/TC-05/11, SLAC-R-773, 2005.
[17] M. Brugger, A. Ferrari, S. Roesler, L. Ulrici, Nuclear Instruments and Methods in Physics Research Section A 562 (2006) 814.
[18] G. Battistoni, A. Ferrari, T. Montaruli, P.R. Sala, Astroparticle Physics 19 (2003) 269;
G. Battistoni, A. Ferrari, T. Montaruli, P.R. Sala, Astroparticle Physics (Erratum) 19 (2003) 291.
[19] S. Maury, Y. Body, O. Brunner, D. Chapuis, J.-P. Corso, C. De Almeida, N. Lopez, S. Prodon, J. Pierlot, LINAC4 Safety File, Technical Report L4-S-SR-0002, EDMS 905423, CERN, Geneva, June 2008.
[20] M. Vretenar, Private communication, CERN, Geneva, 2013.
[21] A. Lombardi, G. Bellodi, V. Dimov, J.-B. Lallement, User Specifications for LINAC4 Dumps—Engineering Parameters (Ref. WP 2.3), Technical Report CERN-L4-T-EP-0006 rev.1.0, EDMS 1184637, CERN, Geneva, June 2012.
[22] E. Mauro, M. Silari, Nuclear Instruments and Methods in Physics Research Section A 605 (3) (2009) 249.
[23] E. Mauro, M. Silari, Residual Dose Rates and Induced Radioactivity in the LINAC4 Tunnel, Technical Report CERN-SC-2008-069-RP-TN, CERN, Geneva, 2008.
[24] P.A. Thonet, LINAC4 Inter-Tank Permanent Magnet Quadrupoles, Technical Report LINAC4 Project Document L4-MQM-ES-0002 rev.1.0, CERN, Geneva, 2012.
[25] I.V. Leitao, C. Maglioni, Design Specifications for the LINAC4 Main Dump, LBE and LBS dumps, Technical Report CERN-L4-T-ES-0007, EDMS 1256894, CERN, Geneva, December 2012.
[26] S. Roesler, C. Theis, Exemption and Clearance of Material at CERN, Technical Report EDMS 942170 v.5, CERN, Geneva, January 2012.
[27] Ordonnance sur la radioprotection (ORaP), Technical Report 814.501, January 2013.
[28] M. Huhtinen, Determination of Cross-Sections for Assessments of Air Activation at LHC, Technical Report CERN/TIS-RP/TM/97-29, CERN, Geneva, 1997.
[29] S. Agosteo, Radiation Protection Dosimetry 137 (1–2) (2009) 167.